

## Evaluation of the Physicochemical Properties and Antiaging Properties of Bitumen Mastic Modified by Layered Double Hydroxides

Zou, Yingxue; Pang, Ling; Chen, Shuaichao ; Xu, S.; Wu, Shaopeng; Amirghanian, Serji; Xu, Haiqin ; Zhao, Zenggang

**DOI**

[10.3390/su15021546](https://doi.org/10.3390/su15021546)

**Publication date**

2023

**Document Version**

Final published version

**Published in**

Sustainability

**Citation (APA)**

Zou, Y., Pang, L., Chen, S., Xu, S., Wu, S., Amirghanian, S., Xu, H., & Zhao, Z. (2023). Evaluation of the Physicochemical Properties and Antiaging Properties of Bitumen Mastic Modified by Layered Double Hydroxides. *Sustainability*, 15(2), Article 1546. <https://doi.org/10.3390/su15021546>

**Important note**

To cite this publication, please use the final published version (if applicable).  
Please check the document version above.

**Copyright**

Other than for strictly personal use, it is not permitted to download, forward or distribute the text or part of it, without the consent of the author(s) and/or copyright holder(s), unless the work is under an open content license such as Creative Commons.

**Takedown policy**

Please contact us and provide details if you believe this document breaches copyrights.  
We will remove access to the work immediately and investigate your claim.

## Article

# Evaluation of the Physicochemical Properties and Antiaging Properties of Bitumen Mastic Modified by Layered Double Hydroxides

Yingxue Zou <sup>1</sup>, Ling Pang <sup>1</sup>, Shuaichao Chen <sup>1</sup>, Shi Xu <sup>2,3,\*</sup> , Shaopeng Wu <sup>1</sup>, Serji Amirkhanian <sup>4</sup>, Haiqin Xu <sup>1</sup> and Zenggang Zhao <sup>1</sup> 

<sup>1</sup> State Key Laboratory of Silicate Materials for Architectures, Wuhan University of Technology, Luoshi Road 122, Wuhan 430070, China

<sup>2</sup> School of Civil Engineering and Architecture, Wuhan University of Technology, Luoshi Road 122, Wuhan 430070, China

<sup>3</sup> Faculty of Civil Engineering and Geosciences, Delft University of Technology, Stevinweg 1, 2628 CN Delft, The Netherlands

<sup>4</sup> Department of Civil Construction and Environmental Engineering, University of Alabama, Tuscaloosa, AL 35487, USA

\* Correspondence: s.xu-1@tudelft.nl

**Abstract:** Layered double hydroxides (LDHs) can shield polymeric materials from UV light, which allows reducing material aging and erosion damage of bituminous pavement under physical and chemical action. In this study, the physicochemical properties, aging resistance, and erosion resistance to the aqueous solution of LDHs modified bitumen mastic (BM) were characterized by Fourier-transform infrared spectroscopy, basic physical tests, viscosity tests, a dynamic shear rheometer, and a bending beam rheometer. The results show that few chemical reactions occurred between LDHs and BM, indicating that a physical mechanism underlay the modification of BM by LDHs. Moreover, LDHs could increase the flow activation energy of BM by 0.12%, increase the high failure temperature from 69.07 °C to 71.07 °C, and decrease the low failure temperature from −10.50 °C to −12.39 °C. Therefore, LDHs could slightly reduce the temperature sensitivity of BM, while slightly enhancing the high and low-temperature rheological properties of BM. Compared with short-term aging and long-term aging, LDHs could significantly improve the UV aging resistance of BM. The above results are consistent with previous studies of LDHs-modified bitumen. Furthermore, water and pH 3 acidic solutions had the greatest degree of erosion to BM, and LDHs could improve the resistance to aqueous solutions. Overall, this study can help to investigate the effects of various environmental factors on the performance of LDHs modified bitumen pavements during long-term use.

**Keywords:** bitumen mastic; layered double hydroxides; aging conditions; water erosion; physicochemical properties; antiaging properties



**Citation:** Zou, Y.; Pang, L.; Chen, S.; Xu, S.; Wu, S.; Amirkhanian, S.; Xu, H.; Zhao, Z. Evaluation of the Physicochemical Properties and Antiaging Properties of Bitumen Mastic Modified by Layered Double Hydroxides. *Sustainability* **2023**, *15*, 1546. <https://doi.org/10.3390/su15021546>

Academic Editor: Ming-Lang Tseng

Received: 18 November 2022

Revised: 7 January 2023

Accepted: 11 January 2023

Published: 13 January 2023



**Copyright:** © 2023 by the authors. Licensee MDPI, Basel, Switzerland. This article is an open access article distributed under the terms and conditions of the Creative Commons Attribution (CC BY) license (<https://creativecommons.org/licenses/by/4.0/>).

## 1. Introduction

Bituminous pavement is used in the natural environment, subjected to the physical and chemical action of heat, light, oxygen, and water and the load of vehicles [1,2]. Thus, the light components of bitumen are easy to volatilize, oxidize, and dissolve, whereby the technical indicators and the rheological properties can deteriorate [3,4]. The properties of bitumen, such as adhesion and fatigue resistance, deteriorate after aging; thus, the water damage resistance and crack resistance of the bitumen mixture are weakened [5,6]. This leads to a series of pavement diseases such as cracking and potholes, which greatly reduce the service life of the bituminous pavement and increase traffic risks [7,8]. The antiaging property is the ability to resist the above reaction, maintain the ratio of light and heavy components in bitumen, and maintain the pavement performance while preventing easy

decay. Therefore, modifying and enhancing the antiaging performance of bituminous pavement can increase its service life, while reducing the maintenance cost of highways and the pollution of solid waste. Bitumen undergoes thermal oxygen aging when it is mixed in a blender [9]. The UV aging of bituminous pavement is easily affected by solar ultraviolet rays during service [10]. In recent years, the focus of highway construction in China has shifted to the western plateau region, where the ozone layer has thinned, exacerbating the UV aging of bituminous pavement. In developed industrial areas, acid rain is frequent, and the bituminous pavement is often corroded by acid rain [11]. The seawater in the southeast coastal area and the saline soil in the northwest area contain a large amount of sodium and sulfate salt, which can cause varying degrees of damage to the bituminous pavement [12,13].

In order to extend the service life of bituminous pavement, antiaging modifiers can be added to bitumen to enhance its aging resistance, which is the most efficient and mature method of bitumen modification [14,15]. Among these, layered double hydroxides (LDHs) can enhance the aging resistance through the physical shield to UV rays [16]. As a layered nanomaterial with a structure similar to brucite, LDHs prolong the penetration distance of oxygen into the bitumen binder to reduce the diffusion of oxygen [17]. The multilayer structure of LDHs can reflect and absorb UV light, making them a good UV shielding material. Thus, LDHs have excellent heat-, light-, and oxygen-blocking abilities and are used as antiaging additives. In recent years, research on LDHs as bitumen antiaging modifiers has also received much attention. He et al. found that LDHs improved the resistance of bitumen to deformation at high temperatures and protected its physicochemical properties, rheological properties, and chemical composition under UV aging [18]. Cao et al. investigated the effect of different particle sizes of LDHs on the UV aging resistance of asphalt using viscosity tests, dynamic shear rheometer (DSR) tests and Fourier-transform infrared spectroscopy (FTIR) tests [19]. Comparing the LDHs with particle sizes of 75 nm, 115 nm and 300 nm, the best modification on the temperature susceptibility and UV-aging resistance of asphalt was achieved with the particle size of 180 nm. Li et al. investigated the effect of dosage of LDHs on the pavement performance and aging resistance of asphalt [20]. They observed that LDHs can improve the high-temperature performance, resistance to thermal oxidative aging and UV aging of bitumen without significantly weakening the other properties of bitumen. They concluded that the dosage of LDHs should be less than 4%. The effect of LDHs on the antiaging performance of bitumen has been thoroughly investigated, and the technology of modifying bitumen with LDHs has gradually matured. However, bituminous concrete is formed by bonding various aggregates with bitumen mastic (BM), which are then condensed together; hence, the antiaging performance of BM directly affects the service life of the bituminous pavement. There are few studies on the physicochemical properties and antiaging performance of LDHs-modified bitumen mastic (MBM).

Therefore, in this study, LDHs MBM was prepared using the melt blending method to evaluate the physicochemical properties and aging resistance of MBM. The effect of LDHs on the properties of BM was investigated, including the chemical structure, physical properties, and rheological properties. Under different aging conditions and different aqueous solutions, the antiaging behavior and anti-solution erosion behavior of LDHs MBM are discussed. The methodological framework was illustrated in Figure 1.

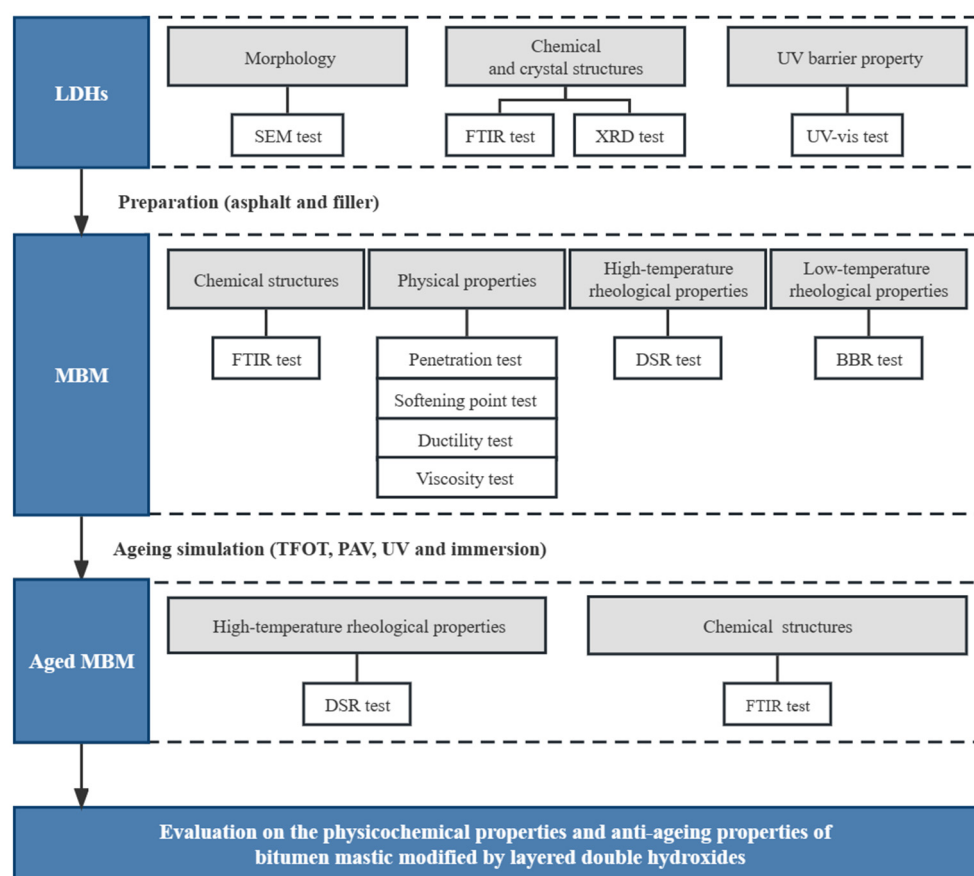


Figure 1. Research program.

## 2. Materials and Experiment

### 2.1. Materials

#### 2.1.1. Bitumen

The PEN 80/100 base bitumen used in this study was produced by Yongte Petrochemical Co., Ltd., Yingkou, Liaoning Province, China. The basic physical performance of the base bitumen was characterized according to relevant specifications, as displayed in Table 1.

Table 1. Physical performance of 80/100 base bitumen.

Physical Performance	Units	Result	Standards
Penetration (25 °C, 100 g, 5 s)	0.1 mm	85.3	ASTM D-5 [21]
Softening point	°C	45.2	ASTM D-36 [22]
Ductility (10 °C)	cm	392	ASTM D-113 [23]
Solubility (trichloroethylene)	%	99.8	ASTM D-2042 [24]

#### 2.1.2. LDHs

As a material with UV aging resistance, LDHs can effectively physically shield and chemically absorb ultraviolet rays, in addition to having good antiaging properties. As the commonly used type of LDHs, the Mg–Al LDH containing interlayer carbonate anions was utilized to modify BM. The basic physical parameters of the Mg–Al LDHs are illustrated in Table 2.

**Table 2.** Basic physical parameters of Mg–Al LDHs [20].

Parameters	Units	LHDs
Ratio of MgO/Al <sub>2</sub> O <sub>3</sub>	/	4.2
Content of LDHs	%	≥99.5
Mass loss (105 °C)	%	≤0.5
Specific surface area	m <sup>2</sup> /g	1.34
Average particle size	μm	5.267

### 2.1.3. Filler

Limestone mineral powder was selected to be the filler, and its technical performance is illustrated in Table 3.

**Table 3.** Technical performance of filler.

Technical Performance	Result	Requirement [25]
Apparent density/g·cm <sup>-3</sup>	2.671	≥2.5
<0.6 mm	100	100
Gradation/wt.%	94.2	90~100
<0.15 mm	81.4	75~100
<0.075 mm	0.62	<1
Hydrophilic coefficient		

### 2.2. Characterization of LDHs

The surface morphology was characterized by scanning electron microscopy (SEM, 139 S3500N type, Hitachi Corp., Tokyo, Japan) with a voltage of 20 kV. Fourier-transform infrared spectroscopy (FTIR, VERTEX 70, Bruker Co., Ltd., Heidelberg, Germany) was utilized to observe the chemical structure within the wave number range of 4000–400 cm<sup>-1</sup> and 64 scans. The crystal structure of LDHs was analyzed by X-ray diffraction (XRD, Bruker AXS D8-Focus, Heidelberg, Germany) with the positive pressure method. The test parameters were a 2θ range of 5°–50° and a scanning rate of 0.25°/s. The diffraction angle in the presence of characteristic peaks could be employed to calculate the interlayer spacing of LDHs using the Bragg equation, as shown in Equation (1) [26].

$$\lambda = 2d \sin \theta, \quad (1)$$

where  $\lambda$  expresses the wavelength of the CuK $\alpha$  ray (equal to 0.15418 nm),  $d$  is the basal spacing between the sheets of LDHs (nm), and  $\theta$  is half of the diffraction angle (°).

UV spectrophotometry (UV/Vis, 750 S 141 PerkinElmer Lambda, Waltham, MA, USA) was carried out to obtain the UV absorbance and reflectance spectra of LDHs within 200–800 nm.

### 2.3. Preparation of BM

The 80 wt.% filler was added to the base bitumen at 150 °C and mixed at 200 rpm for 10 min to obtain the base bitumen mastic (BBM). Additionally, 3 wt.% LDHs were gradually added to the base bitumen in the molten state at 150 °C, and the mixture was stirred at 200 rpm for 30 min. Then, it was sheared at 4000 rpm for 60 min to obtain the LDHs modified bitumen using the melt blending method. Finally, the LDHs-modified bitumen mastic (MBM) was prepared by mixing 80 wt.% filler at 200 rpm for 10 min.

### 2.4. Aging Simulation of BM

The thin-film oven test (TFOT) at 163 °C for 5 h was used to obtain aged BBM and LDHs MBM. Then, the samples were subjected to a pressure aging vessel (PAV) test at 100 °C and 2.1 MPa for 24 h. Additionally, the samples aged by TFOT were placed in the UV aging oven at 40 W/m<sup>2</sup> and 60 °C for 168 h. The unaged BM samples were immersed in five different aqueous solutions, namely, distilled water, pH 3 solution, pH 11 solution,

10 wt.% NaCl solution, and 10 wt.% Na<sub>2</sub>SO<sub>4</sub> solution. The aqueous solution was replaced every other day, and the test was continued for 14 days.

### 2.5. Characterization of BM

Before and after the aging simulation, the chemical structure of BBM and LDHs MBM was characterized by the FTIR spectrum. The bitumen was dissolved in carbon disulfide to form a mixture, which was dripped onto a potassium bromide chip as a test carrier. After the carbon disulfide was completely evaporated, the sample was tested 64 times with a scanning range of 4000–400 cm<sup>-1</sup>. After aging, the indices of the carbonyl group ( $I_{C=O}$ ) and sulfoxide group ( $I_{S=O}$ ) were compared to discuss the aging degree of bitumen, calculated using Equations (2) and (3) [27].

$$I_{C=O} = \frac{A_{\text{around } 1700\text{cm}^{-1}}}{\sum A_{2000-600\text{cm}^{-1}}}, \quad (2)$$

$$I_{S=O} = \frac{A_{\text{around } 1030\text{cm}^{-1}}}{\sum A_{2000-600\text{cm}^{-1}}}, \quad (3)$$

where  $A_{\text{around } 1700\text{cm}^{-1}}$  and  $A_{\text{around } 1030\text{cm}^{-1}}$  represent the 1700 cm<sup>-1</sup> areas centered around C=O and the 1030 cm<sup>-1</sup> areas centered around S=O;  $\sum A_{2000-600\text{cm}^{-1}}$  is the sum of areas from 2000 cm<sup>-1</sup> to 600 cm<sup>-1</sup>.

According to the relevant standards, the penetration, softening point, ductility, and viscosity tests were carried out to analyze the physical properties of BM before aging [21–23,28]. The parameters of the penetration test were a temperature of 25 °C, a weight mass of 100 g, and a test time of 5 s. The ductility test was undertaken at 10 °C. The viscosity test of BM was conducted at 90 °C, 105 °C, 120 °C, 135 °C, and 150 °C. On the basis of the viscosity data, the flow activation energy was obtained through the Arrhenius equation, as shown in Equations (4) and (5) [29].

$$\eta = A \cdot e^{-E_{\eta}/RT}, \quad (4)$$

$$\ln \eta = \ln A - \frac{E_{\eta}}{R} \times \frac{1}{T}, \quad (5)$$

where  $\eta$  represents the viscosity of BM (Pa·s),  $A$  expresses the regression coefficient,  $E_{\eta}$  is the flow activation energy (kJ/mol),  $R$  expresses the universal gas constant (equal to 8.314 J/(mol·K)), and  $T$  represents the test temperature (K). A higher flow activation energy of bitumen mastic indicates a higher viscosity/temperature dependence.

The high-temperature rheological properties of BM were studied using a dynamic shear rheometer (DSR, SmartPave102, Anton Paar Co., Ltd., Berlin, Germany) at 52–76 °C. A rotor diameter of 25 mm and a gap thickness of 1 mm were selected, and the frequency and strain were 10 rad/s and 0.5%, respectively. To discuss the influence of LDHs on antiaging properties, the  $G^*$  aging index (GAI) was defined as the ratio of the  $G^*$  of aged BM to that of unaged BM, calculated using Equation (6) [30].

$$GAI = G_{\text{aged}}^* / G_{\text{unaged}}^* \quad (6)$$

where  $G_{\text{aged}}^*$  and  $G_{\text{unaged}}^*$  are the  $G^*$  of aged and unaged BM respectively, kPa.

The low-temperature rheological properties of BM were characterized using a bending beam rheometer (BBR) test at −6, −12, and −18 °C. The sample was poured with hot bitumen in the mold, forming a rectangular bitumen strip of 127 mm × 12.7 mm × 6.35 mm [31]. The different samples were compared according to the parameters of cracking resistance such as the creep stiffness modulus ( $S$ ) and creep rate ( $m$ -value), calculated using Equations (7) and (8) [32].

$$S(t) = \frac{PL^3}{4bh^3\Delta(t)}, \quad (7)$$

$$m(t) = B + 2C[\lg(t)]^2, \quad (8)$$

where  $S(t)$  is the creep stiffness at 60 s (MPa),  $b$ ,  $h$ , and  $L$  express the width, depth, and span length of the sample (mm),  $\Delta(t)$  expresses the deflection of samples at 60 s,  $P$  is the load (mN), and  $B$  and  $C$  express the regression coefficients between  $\lg[S(t)]$  and  $\lg[m(t)]$ . A lower value of  $S$  indicates better low-temperature ductility [33]. The  $m$ -value represents the change rate of  $S$ , and a larger  $m$ -value indicates a bigger relaxation rate and better low-temperature performance.

### 3. Results and Discussion

#### 3.1. Characterization of LDHs

##### 3.1.1. Morphology

The surface morphology of LDHs was observed using SEM, and the SEM images at  $5000\times$  and  $10,000\times$  magnification are shown in Figure 2a,b, respectively. The surface of LDHs was irregular and uneven in size, and the smooth particles were tightly arranged. The thickness of the thin sheet marked in blue arrow was about 100 nm, whereas the sheet marked in red arrow showed a width of  $1.67\ \mu\text{m}$ . The results were similar to previous studies [27].

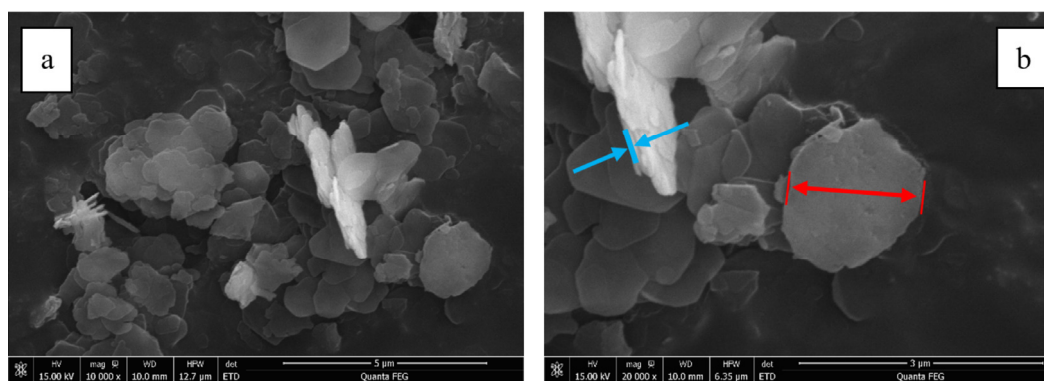


**Figure 2.** SEM images of LDHs (a)  $10,000\times$ ; (b)  $20,000\times$ .

##### 3.1.2. Chemical and Crystal Structures

The chemical structure of LDHs was tested using FTIR, as shown in Figure 3. There were eight characteristic absorption peaks on the infrared spectrum, among which the absorption band at  $3461\ \text{cm}^{-1}$  corresponded to the stretching vibration of  $-\text{OH}$  of the interlayer water. The stretching vibration of the hydrogen bond of  $\text{H}_2\text{O}$  and  $\text{CO}_3^{2-}$  in the interlamellar channels appeared at  $3069\ \text{cm}^{-1}$ . Additionally, the bending vibration of  $\text{H}_2\text{O}$  and asymmetric stretching vibration of  $\text{CO}_3^{2-}$  were present at  $1605\ \text{cm}^{-1}$  and  $1359\ \text{cm}^{-1}$ , respectively. The absorption peaks of  $780\ \text{cm}^{-1}$ ,  $686\ \text{cm}^{-1}$ ,  $550\ \text{cm}^{-1}$ , and  $449\ \text{cm}^{-1}$  were caused by the presence of the metal hydroxide sheets in the magnesium–aluminum lattice, i.e.,  $\text{Al}-\text{O}$ ,  $\text{Mg}-\text{O}$ ,  $\text{O}-\text{Mg}-\text{O}$ , and  $\text{O}-\text{Al}-\text{O}$ . Figure 4 displays the XRD pattern of LDHs, revealing five characteristic peaks of LDHs: 003, 006, 012, 015, and 018. The first three sharp peaks were characteristic of hydrotalcite compounds with diffraction peaks at 34,946, 14,430, and 3488 a.u. This indicated that the LDHs had good preferred orientation and crystal quality [34]. The peaks 003, 006, and 012 corresponded to  $2\theta = 11.60^\circ$ ,  $23.38^\circ$ , and  $34.84^\circ$ , respectively. Their base spacing could be calculated from Equation (1) as 0.76, 0.38, and 0.26 nm, respectively. The characteristic peaks on the FTIR spectra and the crystal structures were recognized in previous studies [20].

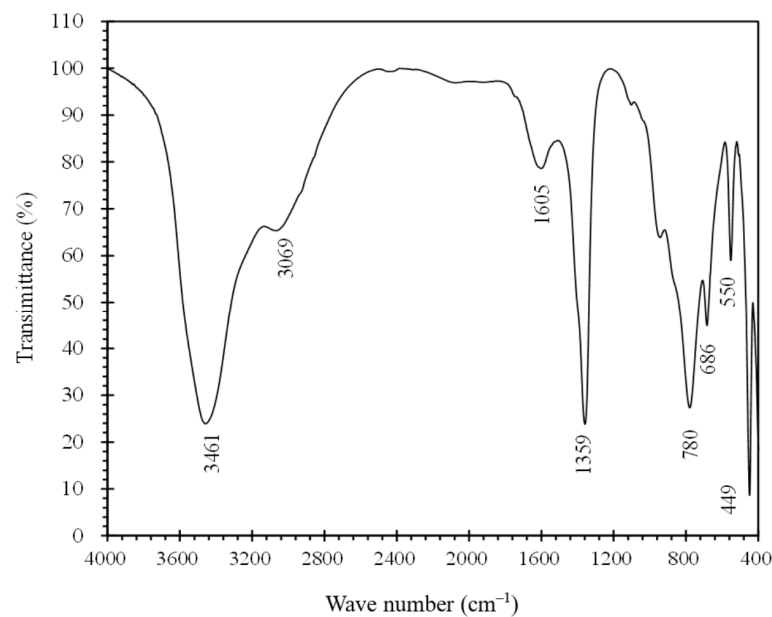


**Figure 3.** The infrared spectrum of LDHs.

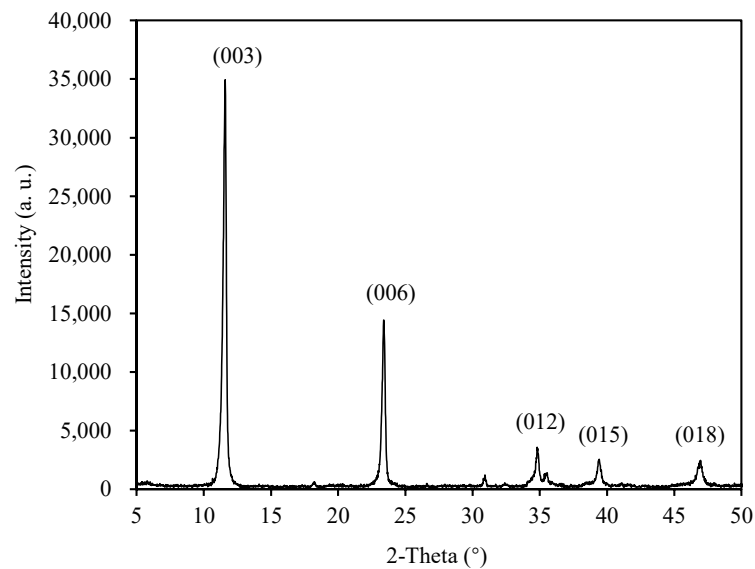


**Figure 4.** XRD pattern of LDHs.

### 3.1.3. UV Barrier Property

The multilayer structure of LDHs enables them to have a UV barrier property, which is the key to their application in bitumen modification. The absorbance and reflectance of LDHs in the UV wavelength range are displayed in Figure 5. The UV reflectance of LDHs increased to 69.41% in the range of 200–230 nm and decreased to a minimum value of 60.74% in the range of 230–256 nm. After 256 nm, the reflectance increased with the increase in wavelength, reaching a peak value of 80.19% in the range of 400 nm. The UV absorbance was opposite to the reflectance and reached the minimum of 0.0916 a.u. at 400 nm. Due to the absorption of UV by the atmosphere, relatively high energy UV can be almost absorbed, and bituminous pavement is mainly affected by UVB (280–315 nm) and UVC (315–400 nm) [35]. LDHs in UV reflection in the range of 280–400 nm was higher than 72.08%, achieving their shielding function. This is close to the UV shielding performance of 88% in a previous study [19]. Therefore, LDHs with UV barrier properties can be utilized as an anti-UV aging additive to enhance the aging resistance of bitumen.

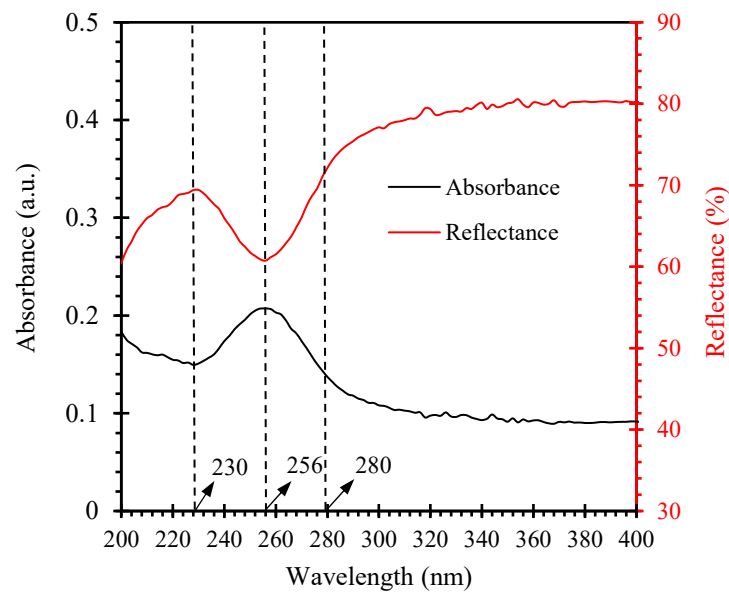


**Figure 5.** UV absorbance and reflectance spectra of LDHs.

### 3.2. Effect of LDHs on Physicochemical Properties of BM

#### 3.2.1. Chemical Structure

To investigate the influence of LDHs on the chemical structure of BM, the FTIR spectra of BM before and after the addition of LDHs are shown in Figure 6. The corresponding characteristic peaks in the BM spectra are  $2924\text{ cm}^{-1}$ ,  $2853\text{ cm}^{-1}$ , and  $1458\text{ cm}^{-1}$ , corresponding to C–H. In addition, the peaks at  $1601$ ,  $1377$ , and  $733\text{ cm}^{-1}$  correspond to an asymmetrically substituted benzene ring, methyl group, and aromatic branch chain. Eight characteristic absorption peaks of LDHs could be observed on the spectrum of LDHs MBM, and no new characteristic peaks appeared on LDHs MBM. This suggested that there was no chemical reaction between LDHs and BM, and that the modification of BM by LDHs was a physical method, just like the modification of bitumen by LDHs [36].

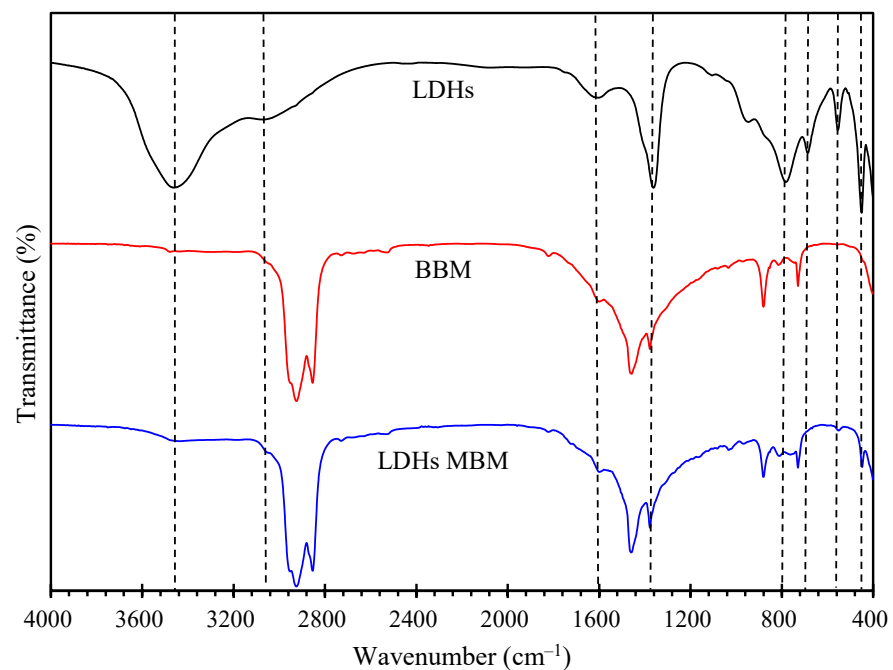


**Figure 6.** FTIR spectrum of LDHs, BBM, and LDHs MBM.

### 3.2.2. Physical Properties

The physical properties of BM are related to the machining and road performance of bituminous concrete [37]. Table 4 compares the physical properties of BBM and LDHs MBM. After modification, the softening point of LDHs MBM increased by 4.81%, while the penetration and ductility decreased by 5.23% and 3.17%, respectively. This manifests that LDHs hardened the BM and improved the high-temperature performance, while they weakened the low-temperature performance. This is because inorganic nanomaterial LDHs block the free movement of bitumen molecule chains in the BM [38].

**Table 4.** Physical properties of BBM and LDHs MBM.

Physical Properties	Units	BBM	LDHs MBM	Variation (%)
Penetration (25 °C, 100 g, 5 s)	0.1 mm	59.3	56.2	−5.23
Softening point	°C	49.9	52.3	4.81
Ductility (10 °C)	cm	221	214	−3.17

The viscosity of BM can reflect the deformation of BM from a viscoelastic to a viscous–fluid state over a wide temperature region, which indirectly characterizes the temperature sensitivity of bitumen and the workability of bituminous concrete [39]. Figure 7 illustrates the viscosity of BBM and LDHs MBM at 90 °C, 105 °C, 120 °C, 135 °C, and 150 °C. It can be seen that the viscosity of BBM and LDHs MBM decreased with the increase in temperature. The addition of LDHs increased the viscosity of BM by 13.68%, 16.57%, 17.24%, 17.07%, and 12.50% at 90 °C, 105 °C, 120 °C, 135 °C, and 150 °C, respectively.

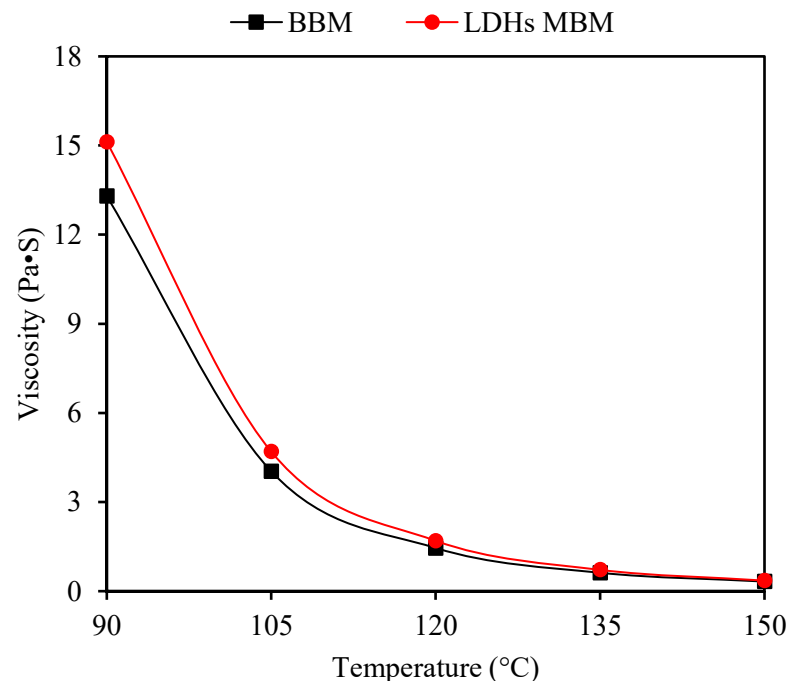


**Figure 7.** Viscosity–temperature curve of BBM and LDHs MBM.

The viscosity–temperature curves for all samples were fitted to the Arrhenius Equations (2) and (3), as displayed in Figure 8. The fitted parameters are shown in Table 5. The fitting results showed that the correlation coefficients ( $R^2$ ) of BBM and LDHs MBM were 0.9955 and 0.9968, respectively, both reaching 0.99. Therefore, the Arrhenius equation could better describe the viscosity–temperature relationship of LDHs MBM. The addition of LDHs increased  $\eta$  by 0.12% compared to the base BM, and the activation energy required for the conversion of BM to the viscoelastic state increased slightly. This indicates that the addition of 3% LDHs had little effect on temperature sensitivity. The effect of LDHs

on bitumen mastic was smaller than the effect of LDHs on the temperature sensitivity of bitumen [19]. The fitted viscosity–temperature relationship could provide a reliable basis for the determination of mixing and compaction temperatures of bitumen mixture [29].

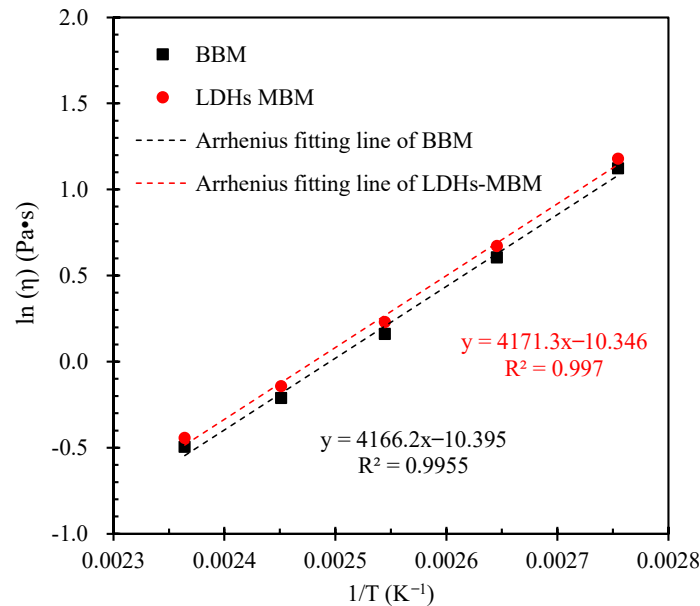


Figure 8. Arrhenius fitting lines of BBM and LDHs MBM.

Table 5. The fitting parameters of samples.

Mastic	Fitting Line	R <sup>2</sup>	Slope (−E <sub>η</sub> /R)	E <sub>η</sub>   (kJ/mol)
BBM	y = 4166.2x − 10.395	0.9955	4166.2	34.6378
LDHs MBM	y = 4171.3x − 10.346	0.9970	4171.3	34.6802

### 3.2.3. High-Temperature Rheological Properties

$G^*$  and  $\delta$  are considered parameters characterizing the rheological properties at high temperatures. A larger  $G^*$  indicates a higher shear resistance, and vice versa [40]. The value of  $\delta$  can be used to calculate the ratio of the elastic component to the viscous component. A larger  $\delta$  indicates a more viscous component. On the contrary, a smaller  $\delta$  indicates a more elastic component. It can be seen from Figure 9 that the addition of LDHs increased the  $G^*$  and decreased the  $\delta$  of BM, indicating that LDHs could improve the shear deformation resistance of BM and increase the elastic component of BM. The rutting resistance factor is usually characterized by  $G^*/\sin\delta$  [40]. A higher value denotes better rutting resistance. As can be seen from Figure 10, the rutting factor of LDHs MBM was greater than that of BBM, indicating that the rutting resistance was improved. The SHRP program specifies that the failure temperature was determined by the temperature at  $G^*/\sin\delta = 1$  kPa. According to Figure 10, the failure temperature of BBM was 69.07 °C and the failure temperature of MBM with LDHs was 71.07 °C. LDHs could improve the high-temperature rheological properties of BM, consistent with the physical property test results. The effect of LDHs on the high-temperature rheological properties of BM was less than that on the high-temperature rheological properties of bitumen [18]. This might be due to the addition of fillers that weakened the effect.

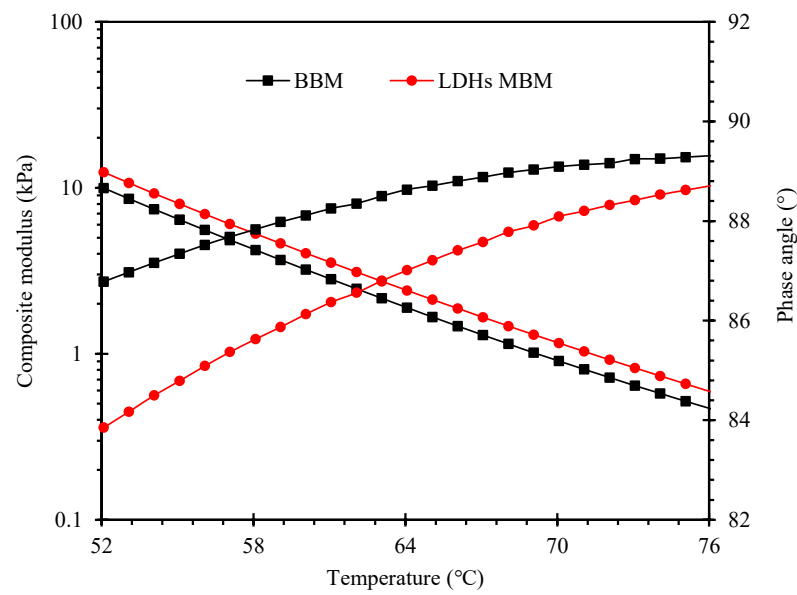


Figure 9.  $G^*$  and  $\delta$  of BBM and LDHs MBM.

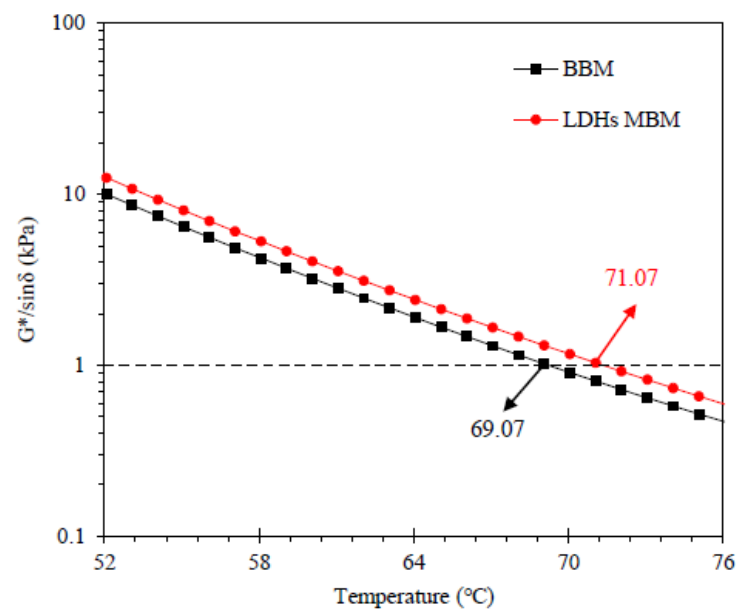


Figure 10.  $G^*/\sin\delta$  of BBM and LDHs MBM.

### 3.2.4. Low-Temperature Rheological Properties

The low-temperature rheological properties of BBM and LDHs-BBM were characterized by the  $S$  and  $m$  values obtained from the BBR test, as shown in Figure 11. As the test temperature decreased, the  $S$  value gradually increased, and the  $m$  value gradually decreased. The results show that the ductility and relaxation rate of BM gradually decreased at low temperatures, and BM became stiff and brittle. The addition of LDHs decreased the  $S$  of BM at  $-6$  °C and  $-12$  °C and increased the  $S$  at  $-18$  °C. The  $m$  value increased at three different temperatures after modification. In general, a lower  $S$  value indicates better ductility at low temperature [33]. A higher  $m$  value indicates a higher relaxation rate and better low-temperature properties. The data suggest that LDHs improved the low-temperature properties of BM at  $-6$  °C and  $-12$  °C. While the regularities of  $S$  and  $m$  values were not inconsistent at  $-18$  °C, a new index  $k = m/S$  was introduced to uniformly evaluate the low-temperature properties of BM [41]. A higher  $k$  denotes better low-temperature properties of BM; the results are shown in Figure 12. Compared with BBM, the  $k$  values of

LDHs MBM at  $-6\text{ }^{\circ}\text{C}$ ,  $-12\text{ }^{\circ}\text{C}$ , and  $-18\text{ }^{\circ}\text{C}$  were improved by 1.33, 1.18, and 1.42 times, respectively. This manifests that LDHs could improve the low-temperature properties of BM. To study the low-temperature properties of BM, it was also necessary to study the failure temperature of BM at low temperatures. According to BBR test results,  $S$  and  $m$  values at different temperatures were fitted linearly as shown in Figure 11 [32]. The  $R^2$  value was close to or greater than 0.9, indicating that the fitting data could offer a reliable reliability of low-temperature failure. According to the fitting formula, the failure temperature of BBM and LDHs MBM was  $-10.50\text{ }^{\circ}\text{C}$  and  $-12.39\text{ }^{\circ}\text{C}$ , respectively. Therefore, LDHs could improve the low-temperature rheological properties of BM.

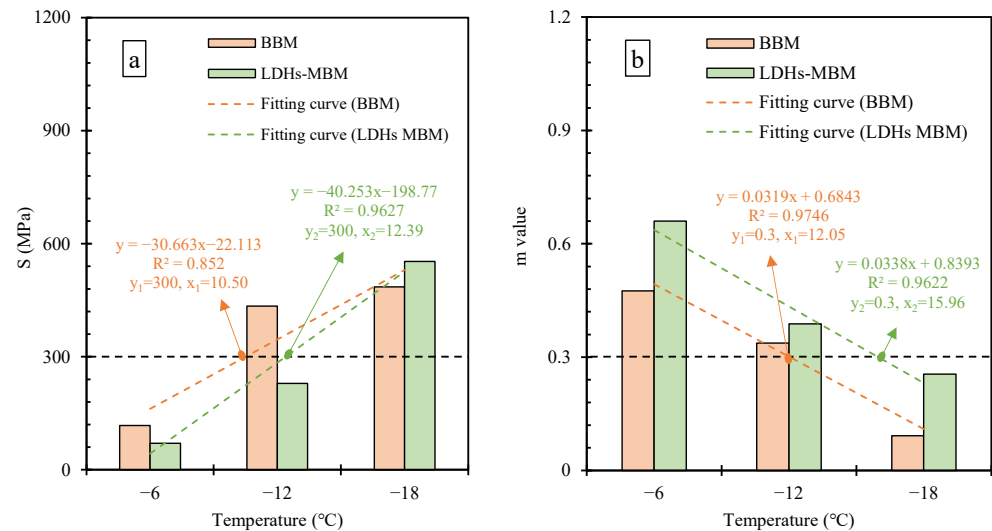


Figure 11.  $S$  (a) and  $m$ -value (b) of BBM and LDHs MBM.

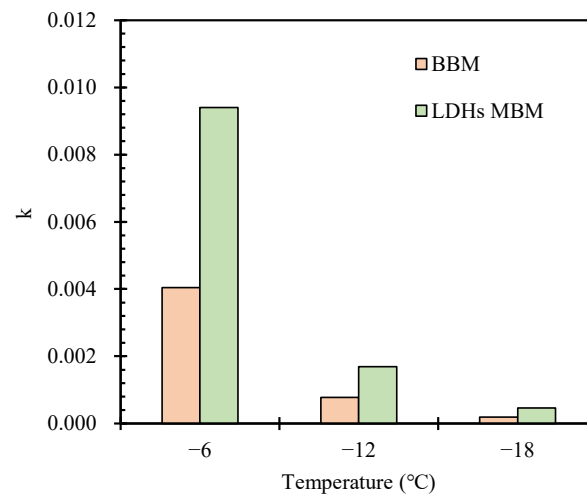


Figure 12.  $k$  of BBM and LDHs MBM.

### 3.3. Effect of LDHs on Antiaging Properties of BM

#### 3.3.1. Effect of LDHs on GAI of BM

BM is a viscoelastic mixture that is plastic at high temperatures and prone to irrecoverable deformation [42]. To explore the influence of different aging conditions on the rheological properties of LDHs MBM, Figure 13a compares the  $G^*$  of BBM and LDHs MBM with different aging degrees. Aging increased the  $G^*$  of BM in the order of TFOT < PAV < UV. The addition of LDHs increased the  $G^*$  of the unaged BM and BM aged by TFOT and PAV, while the  $G^*$  of UV-aged samples was smaller than that of UV-aged BBM. Figure 13b illustrates the GAI of BM under different aging conditions. Compared to the BBM, the GAI

of LDHs MBM was greater after TFOT and PAV aging, while it was smaller after UV aging. This suggests that the addition of LDHs increased the  $G^*$  of BM and hardened BM, making it more susceptible to TFOT and PAV. However, the UV barrier property of LDHs and the UV aging resistance of BM were successfully enhanced. This was the same result as for LDHs-modified bitumen [43].

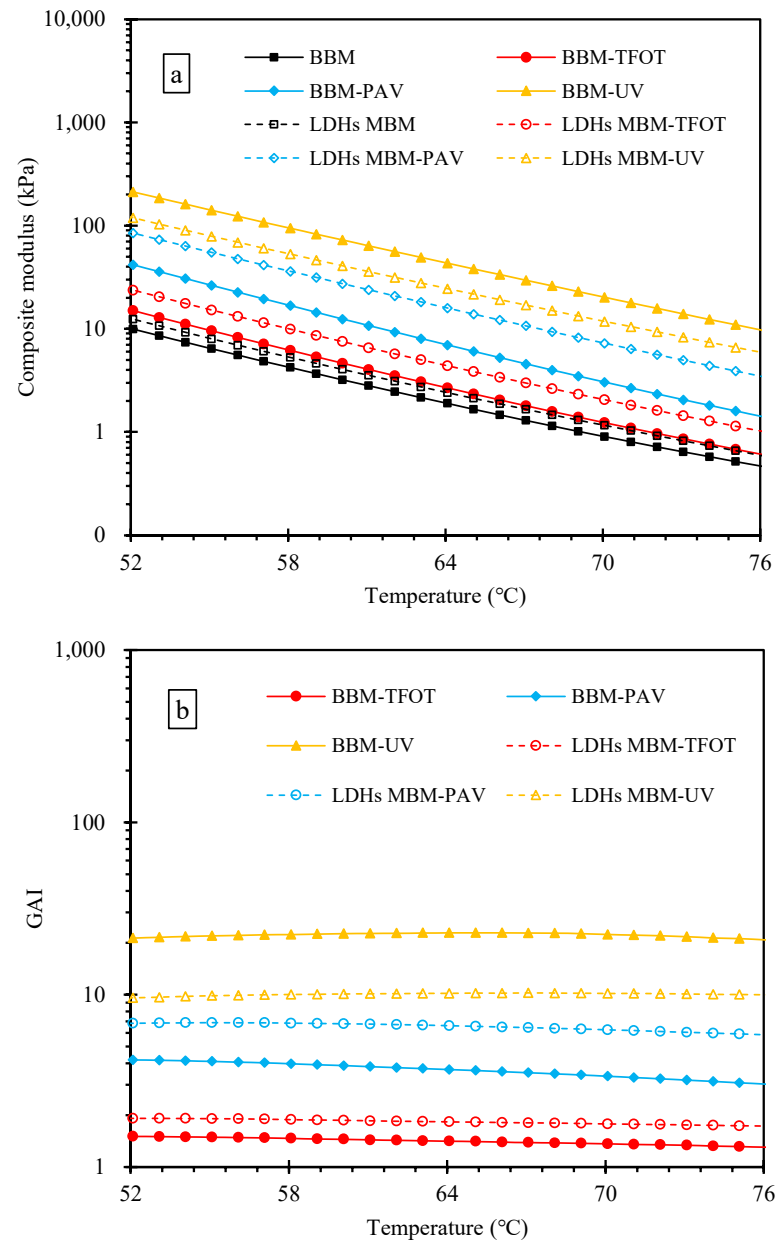


**Figure 13.**  $G^*$  (a) and GAI (b) of BBM and LDHs MBM with different aging degrees.

The  $G^*$  of BM after immersion in different solutions is displayed in Figure 14a. The reduction in  $G^*$  of BBM after immersion was in the order of  $H_2O < pH\ 3 < NaCl < Na_2SO_4 < pH\ 11$ . The  $G^*$  of LDHs MBM was  $pH\ 3 < H_2O < NaCl < Na_2SO_4 < pH\ 11$ . For LDHs MBM, the reduction in  $G^*$  after immersion was less than that of BBM. Figure 14b compares the GAI of BBM and LDHs MBM after immersion in different solutions. Because the solution erosion reduced the  $G^*$  of BM, the GAI was less than 1. Thus, a smaller GAI indicated a greater degree of erosion at this time. It can be seen from the figure that the GAI of LDHs MBM was larger than that of BBM after immersion in different aqueous solutions, indicating that the addition of LDHs improved the resistance of BM to the aqueous solution.

It might be that the layered structure of LDHs led to a longer penetration distance of the aqueous solution, which acted as a shielding effect.

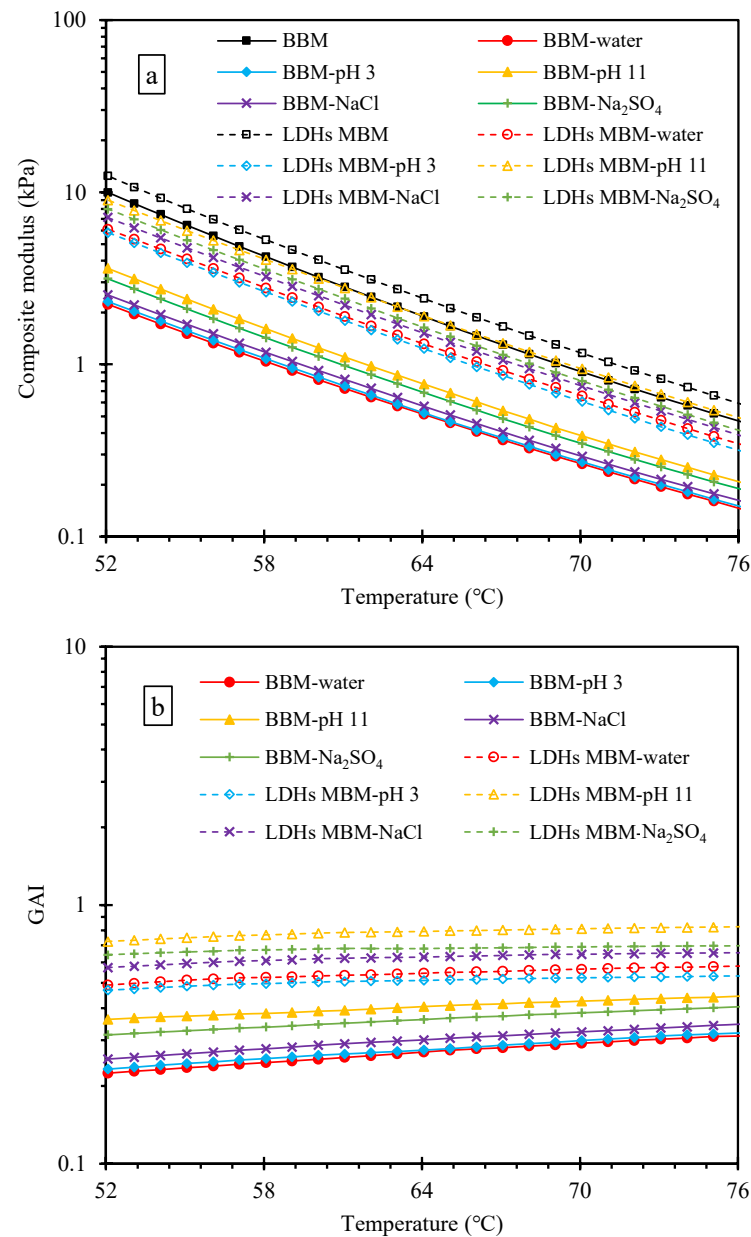


**Figure 14.**  $G^*$  (a) and GAI (b) of BBM and LDHs MBM immersed in different solutions.

### 3.3.2. Effect of LDHs on $I_{C=O}$ and $I_{S=O}$ of BM

The effects of different aging conditions on BBM and LDHs MBM were further investigated using  $I_{C=O}$  and  $I_{S=O}$  as aging indicators. Figure 15 shows the effect of TFOT, PAV, and UV aging on the chemical structure of BBM and LDHs MBM. According to the figure, the  $I_{C=O}$  of BBM and LDHs MBM gradually increased under various aging conditions. Furthermore, the  $I_{S=O}$  gradually increased after TFOT and PAV aging, while the  $I_{S=O}$  after UV aging was smaller than that after PAV aging. The  $I_{C=O}$  and  $I_{S=O}$  of LDHs MBM were smaller than those of BBM under various ageing conditions, especially for UV aging. Compared with BBM after UV aging, the  $I_{C=O}$  and  $I_{S=O}$  of LDHs MBM were reduced by 57.12% and 35.10%, respectively. This shows that LDHs could effectively improve the resistance of BM to TFOT, PAV, and UV aging, and the improvement effect of resistance to UV aging was the most significant. Previous studies showed a similar effect of LDHs on  $I_{C=O}$  and  $I_{S=O}$  of bitumen after aging [27].

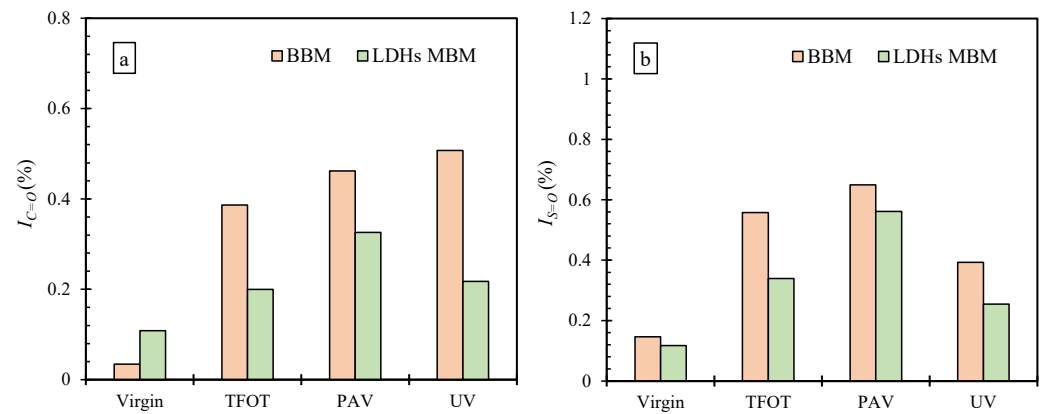


**Figure 15.**  $I_{C=O}$  (a) and  $I_{S=O}$  (b) of BBM and LDHs MBM under different ageing conditions.

The influence of different aqueous solutions on the  $I_{C=O}$  and  $I_{S=O}$  is illustrated in Figure 16, and the change rate based on BM without immersion was calculated (Table 6). The  $I_{C=O}$  of BBM increased after erosion MBM in water and pH 3, but decreased after immersion in pH 11, NaCl, and  $\text{Na}_2\text{SO}_4$ . The rate of change was the largest after water erosion, which increased by 10.41 times. The change degree of  $I_{C=O}$  was greatly reduced by 0.14 after water erosion. After the addition of LDHs, the change degree of  $I_{C=O}$  after immersion in aqueous solutions other than NaCl solution was also reduced. The  $I_{S=O}$  increased after erosion by different aqueous solutions, and the maximum change rate increased by 1.52 times after erosion by an alkali solution. The erosion degree of water and  $\text{Na}_2\text{SO}_4$  was unchanged after the addition of LDHs. At the same time, the erosion degree of pH 3 and pH 11 was reduced, and the erosion degree of NaCl was doubled. This shows that LDHs could improve the resistance to water, pH 3, pH 11, and  $\text{Na}_2\text{SO}_4$ , but weaken the resistance to NaCl erosion.

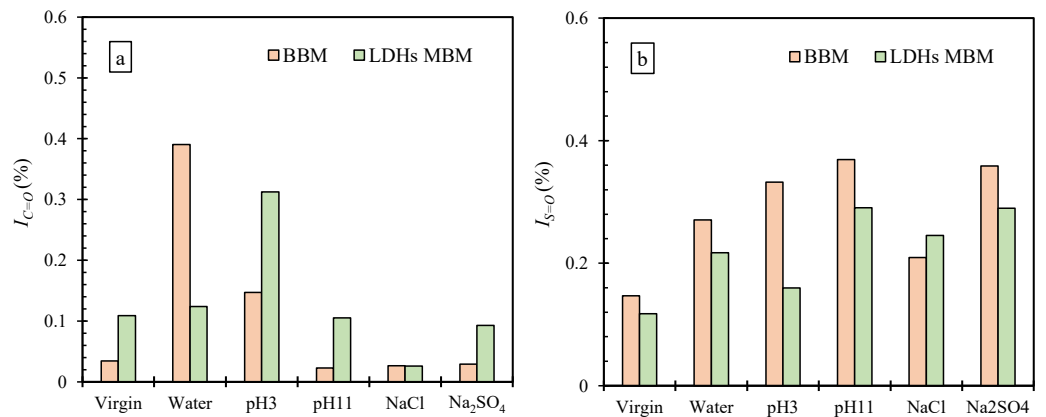


**Figure 16.**  $I_{C=O}$  (a) and  $I_{S=O}$  (b) of BBM and LDHs immersed in different aqueous solutions.

**Table 6.** Change rate of  $I_{C=O}$  and  $I_{S=O}$  based on BM without immersion (times).

Sample	$I_{C=O}$		$I_{S=O}$	
	BBM	LDHs MBM	90 M	LDHs MBM
Water	10.41	0.14	0.84	0.85
pH 3	3.29	1.88	1.27	0.36
pH 11	−0.34	−0.03	1.52	1.47
NaCl	−0.24	−0.76	0.43	1.09
$\text{Na}_2\text{SO}_4$	−0.15	−0.14	1.45	1.47

#### 4. Conclusions

LDHs -MBM was characterized by FTIR, physical properties test, viscosity test, DSR, and BBR to discuss the physicochemical properties. The antiaging properties of LDHs-

MBM were evaluated by GAI,  $I_{C=O}$  and  $I_{S=O}$ , TFOT, PAV, UV aging, and immersion in aqueous solution. The following conclusions can be drawn:

- There were few chemical reactions between the LDHs and BM; thus, the modification of BM by LDHs is a physical method.
- In terms of physical properties, LDHs could improve the high-temperature performance and weaken the low-temperature performance. Additionally, LDHs could increase the viscosity of BM, increasing  $\eta$  by 0.12%, indicating that LDHs could slightly reduce the temperature sensitivity of BM.
- LDHs enhanced the high failure temperature of BM from 69.07 °C to 71.07 °C and reduce the low failure temperature from −8.83 °C to −13.61 °C. Therefore, LDHs could improve the high-temperature and low-temperature rheological properties of BM.
- The addition of LDHs increased the  $G^*$  of BM and hardened BM, making the rheological properties more susceptible to the effects of TFOT and PAV aging. Nevertheless, LDHs could slow the formation of carbonyl and sulfoxide groups during TFOT and PAV aging. This shows that LDHs could improve the resistance of BM to TFOT and PAV aging to a certain extent. Due to the UV barrier property of LDHs, the UV aging resistance of BM was successfully enhanced.
- The GAI of BBM decreased after immersion in the order of  $H_2O < pH\ 3 < NaCl < Na_2SO_4 < pH\ 11$ . The addition of LDHs can enhance the GAI of BM immersed in various aqueous solutions. The erosion of different aqueous solutions on BM decreased in the order of erosion degree as follows:  $H_2O > pH\ 3 > pH\ 11 > NaCl > Na_2SO_4$ . After the addition of LDHs, the change degree of  $I_{C=O}$  and  $I_{S=O}$  was greatly reduced after immersion in an aqueous solution except for NaCl solution. Combining the results of GAI,  $I_{C=O}$ , and  $I_{S=O}$  indicates that water and pH 3 had the greatest degree of erosion to BM, and LDHs could improve the resistance to five kinds of an aqueous solution.

This study is conducive to investigating the performance degradation of LDHs-modified bituminous pavement under various environmental factors during long-term service, and it is committed to the promotion of LDHs in pavement engineering. In the FTIR test, the addition of LDHs increased the  $I_{C=O}$  and  $I_{S=O}$  of BM after immersion in NaCl solution. In future research, the erosion behavior of NaCl on LDHs -modified bitumen will be further investigated.

**Author Contributions:** Y.Z., methodology, investigation, and writing—original draft; L.P., conceptualization and validation; S.C., data curation and formal analysis; S.X., investigation and writing—review and editing; S.W., conceptualization and supervision; S.A., methodology and supervision; H.X., visualization and software; Z.Z., methodology and validation. All authors have read and agreed to the published version of the manuscript.

**Funding:** This research was sponsored by the National Natural Science Foundation of China [52108416] and the Independent Innovation Foundation of Wuhan University of Technology [223131001].

**Institutional Review Board Statement:** Not applicable.

**Informed Consent Statement:** Not applicable.

**Data Availability Statement:** The data presented in this study are available on request from the corresponding author.

**Conflicts of Interest:** The authors declare no conflict of interest.

## References

1. Zhang, L.; Hoff, I.; Zhang, X.; Yang, C. Investigation of the self-healing and rejuvenating properties of aged asphalt mixture containing multi-cavity Ca-alginate capsules. *Constr. Build. Mater.* **2022**, *361*, 129685. [[CrossRef](#)]
2. Wan, P.; Wu, S.; Liu, Q.; Wang, H.; Zhao, F.; Wu, J.; Niu, Y.; Ye, Q. Sustained-release calcium alginate diatomite capsules for sustainable self-healing asphalt concrete. *J. Clean. Prod.* **2022**, *372*, 133639. [[CrossRef](#)]
3. Yan, S.; Zhou, C.; Ouyang, J. Rejuvenation effect of waste cooking oil on the adhesion characteristics of aged asphalt to aggregates. *Constr. Build. Mater.* **2022**, *327*, 126907. [[CrossRef](#)]

4. Xu, H.; Wu, S.; Chen, A.; Zou, Y. Influence of erosion factors (time, depths and environment) on induction heating asphalt concrete and its mechanism. *J. Clean. Prod.* **2022**, *363*, 132521. [[CrossRef](#)]
5. Yang, C.; Wu, S.; Cui, P.; Amirkhanian, S.; Zhao, Z.; Wang, F.; Xie, J. Performance characterization and enhancement mechanism of recycled asphalt mixtures involving high RAP content and steel slag. *J. Clean. Prod.* **2022**, *336*, 130484. [[CrossRef](#)]
6. Xu, Z.; Wang, Y.; Cao, J.; Chai, J.; Cao, C.; Si, Z.; Li, Y. Adhesion between asphalt molecules and acid aggregates under extreme temperature: A ReaxFF reactive molecular dynamics study. *Constr. Build. Mater.* **2021**, *285*, 122882. [[CrossRef](#)]
7. Cui, P.; Wu, S.; Xiao, Y.; Hu, R.; Yang, T. Environmental performance and functional analysis of chip seals with recycled basic oxygen furnace slag as aggregate. *J. Hazard. Mater.* **2021**, *405*, 124441. [[CrossRef](#)]
8. Xu, H.; Wu, S.; Chen, A.; Zou, Y.; Yang, C.; Cui, P. Study on preparation and characterization of a functional porous ultra-thin friction course (PUFC) with recycled steel slag as aggregate. *J. Clean. Prod.* **2022**, *380*, 134983. [[CrossRef](#)]
9. Yang, J.; Zhang, Z.; Shi, J.; Yang, X.; Fang, Y. Comparative analysis of thermal aging behavior and comprehensive performance of high viscosity asphalt (HVA) from cohesion, adhesion and rheology perspectives. *Constr. Build. Mater.* **2022**, *317*, 125982. [[CrossRef](#)]
10. Li, J.; Yu, J.; Wu, S.; Xie, J. The mechanical resistance of asphalt mixture with steel slag to deformation and skid degradation based on laboratory accelerated heavy loading test. *Materials* **2022**, *15*, 911. [[CrossRef](#)]
11. Xie, Q.; Ling, X.; Orji, J.; Onu, E. Evaluation of sustainable acid rain control options utilizing a fuzzy TOPSIS multi-criteria decision analysis model frame work. *J. Clean. Prod.* **2017**, *141*, 612–625.
12. Zhang, J.; Lai, Y.; Li, J.; Zhao, Y. Study on the influence of hydro-thermal-salt-mechanical interaction in saturated frozen sulfate saline soil based on crystallization kinetics. *Int. J. Heat Mass Tran.* **2020**, *146*, 118868. [[CrossRef](#)]
13. Xu, O.; Yang, X.; Xiang, S.; Zhang, H. Migration characteristic and model of chloride ions for NaCl-based salt storage asphalt mixtures. *Constr. Build. Mater.* **2021**, *280*, 122482. [[CrossRef](#)]
14. Zhang, D.; Chen, Z.; Zhang, H.; Wei, C. Rheological and anti-aging performance of SBS modified asphalt binders with different multi-dimensional nanomaterials. *Constr. Build. Mater.* **2018**, *188*, 409–416. [[CrossRef](#)]
15. Ren, S.; Liu, X.; Wang, H.; Fan, W.; Erkens, S. Evaluation of rheological behaviors and anti-aging properties of recycled asphalts using low-viscosity asphalt and polymers. *J. Clean. Prod.* **2020**, *253*, 120048. [[CrossRef](#)]
16. Xu, E.; Chen, P.; Wang, G.; Li, K.; Lin, Y. A facile approach to enhancing the UV blocking properties of layered double hydroxides and potential application in asphalt. *Mater. Today Sustain.* **2021**, *14*, 100081. [[CrossRef](#)]
17. He, B.; Xiao, Y.; Li, Y.; Fu, M.; Yu, J.; Zhu, L. Preparation and characterization of lignin grafted layered double hydroxides for sustainable service of bitumen under ultraviolet light. *J. Clean. Prod.* **2022**, *350*, 131536. [[CrossRef](#)]
18. He, B.; Yu, J.; Yi, G.; Zhuang, R.; Sun, Y. Rheological properties of lignosulfonate intercalated layered double hydroxides modified bitumen before and after ultraviolet aging. *Constr. Build. Mater.* **2018**, *180*, 342–350. [[CrossRef](#)]
19. Cao, Z.; Chen, M.; He, B.; Han, X.; Yu, J.; Xue, L. Investigation of ultraviolet aging resistance of bitumen modified by layered double hydroxides with different particle sizes. *Constr. Build. Mater.* **2019**, *196*, 166–174. [[CrossRef](#)]
20. Li, Y.; Wu, S.; Pang, L.; Liu, Q.; Wang, Z.; Zhang, A. Investigation of the effect of Mg-Al-LDH on pavement performance and aging resistance of styrene-butadiene-styrene modified asphalt. *Constr. Build. Mater.* **2018**, *172*, 584–596. [[CrossRef](#)]
21. *ASTM D-5*; Standard Test Method for Penetration of Bituminous Materials. ASTM International: West Conshohocken, PA, USA, 1992.
22. *ASTM D-36*; Standard Test Method for Softening Point of Bitumen (Ring-and-Ball Apparatus). ASTM International: West Conshohocken, PA, USA, 2009.
23. *ASTM D-113*; Standard Test Method for Ductility of Bituminous Materials. ASTM International: West Conshohocken, PA, USA, 2007.
24. *ASTM D-2042*; Standard Test Method for Solubility of Asphalt Materials in Trichloroethylene. ASTM International: West Conshohocken, PA, USA, 2015.
25. *JTG E20-2011*; Standard Test Methods of Bitumen and Bituminous Mixtures for Highway Engineering. Ministry of Transport of the People's Republic of China: Beijing, China, 2011.
26. Vargas, M.A.; Moreno, L.; Montiel, R.; Manero, O.; Vázquez, H. Effects of montmorillonite (Mt) and two different organo-Mt additives on the performance of asphalt. *Appl. Clay Sci.* **2017**, *139*, 20–27. [[CrossRef](#)]
27. Chen, S.; Liu, Q.; Wu, H.; Yang, C.; Gong, X.; Wu, S.; Li, Y. Simultaneous enhancement of the thermal oxygen and ultraviolet aging resistance of asphalt by incorporating antioxidant intercalated layered double hydroxide. *Constr. Build. Mater.* **2022**, *349*, 128743. [[CrossRef](#)]
28. *ASTM D4402-06*; Standard Test Method for Viscosity Determination of Asphalt at Elevated Temperatures Using a Rotational Viscometer. ASTM International: West Conshohocken, PA, USA, 2006.
29. Yang, C.; Wu, S.; Xie, J.; Amirkhanian, S.; Zhao, Z.; Xu, H.; Wang, F.; Zhang, L. Development of blending model for RAP and virgin asphalt in recycled asphalt mixtures via a micron-Fe<sub>3</sub>O<sub>4</sub> tracer. *J. Clean. Prod.* **2023**, *383*, 135407. [[CrossRef](#)]
30. Zhu, C.; Zhang, H.; Zhang, D.; Chen, Z. Influence of base asphalt and SBS modifier on the weathering aging behaviors of SBS modified asphalt. *J. Mater. Civ. Eng.* **2018**, *30*, 04019184. [[CrossRef](#)]
31. *ASTM D6648-08*; Standard Test Method for Determining the Flexural Creep Stiffness of Asphalt Binder Using the Bending Beam Rheometer (BBR). ASTM International: West Conshohocken, PA, USA, 2016.

32. Ren, H.; Qian, Z.; Huang, W.; Li, H.; Liu, Y. Low-temperature thermal cracking performance of waterborne epoxy asphalt emulsion mastic based on bending beam rheometer (BBR). *Constr. Build. Mater.* **2022**, *334*, 127461. [[CrossRef](#)]
33. Garilli, E.; Autelitano, F.; Giuliani, F. Use of bending beam rheometer test for Theological analysis of asphalt emulsion-cement mastics in cold in-place recycling. *Constr. Build. Mater.* **2019**, *222*, 484–492. [[CrossRef](#)]
34. Wu, Z.; Qu, Y.; Zhang, W.; Xie, G.; Li, Y.; Shen, Q.; Yu, X. Electrochemical properties of Zn-Al-La layered double hydroxides in Zn-Ni secondary batteries. *ACS Omega* **2021**, *6*, 35244–35249. [[CrossRef](#)]
35. Quilez-Molina, A.I.; Marini, L.; Athanassiou, A.; Bayer, I.S. UV-blocking, transparent, and antioxidant polycyanoacrylate films. *Polymers* **2020**, *12*, 2011. [[CrossRef](#)]
36. Zhang, C.; Yu, J.; Xue, L.; Sun, Y. Investigation of  $\gamma$ -(2,3-epoxypropoxy) propyltrimethoxy silane surface modified layered double hydroxides improving UV ageing resistance of asphalt. *Materials* **2017**, *10*, 78. [[CrossRef](#)]
37. Zhang, J.; Li, P.; Sun, C.; Liang, M.; Li, Y.; Yao, Z.; Zhang, X. Effects of composite warm mix additive (CAR) on the physical and rheological performance of bitumen and the pavement performance of its concrete. *Materials* **2019**, *12*, 3916. [[CrossRef](#)]
38. Manias, E.; Touny, A.; Wu, L.; Strawhecker, K.; Lu, B.; Chung, T.C. Polypropylene/Montmorillonite Nanocomposites. Review of the Synthetic Routes and Materials Properties. *Am. Chem. Soc.* **2001**, *13*, 3516–3523. [[CrossRef](#)]
39. Saboo, N.; Singh, B.; Kumar, P.; Vikram, D. Study on viscosity of conventional and polymer modified asphalt binders in steady and dynamic shear domain. *Mech. Time-Depend. Mat.* **2018**, *22*, 67–78. [[CrossRef](#)]
40. Ren, H.; Qian, Z.; Huang, W.; Li, H.; Liu, G. High-temperature rheological properties of waterborne epoxy asphalt emulsion mastic. *Constr. Build. Mater.* **2022**, *325*, 126796. [[CrossRef](#)]
41. Liu, S.; Cao, W.; Shang, S.; Hui, Q.; Fang, J. Analysis and application of relationships between low-temperature rheological performance parameters of asphalt binders. *Constr. Build. Mater.* **2010**, *24*, 471–478. [[CrossRef](#)]
42. Li, Y.; He, X.; Sun, H.; Tan, Y. Research on viscoelastic-plastic damage characteristics of cement asphalt composite binder. *Constr. Build. Mater.* **2021**, *274*, 122064. [[CrossRef](#)]
43. Gu, M.; Zhang, T.; Zhu, K.; Tang, D.; Ke, W.U. Effect of Various Metal Hydroxide Flame Retardants on the Rheological Properties of Asphalt Binder. *Mater. Sci.* **2019**, *25*, 348–355. [[CrossRef](#)]

**Disclaimer/Publisher's Note:** The statements, opinions and data contained in all publications are solely those of the individual author(s) and contributor(s) and not of MDPI and/or the editor(s). MDPI and/or the editor(s) disclaim responsibility for any injury to people or property resulting from any ideas, methods, instructions or products referred to in the content.